Inorganic Chemistry

ARTICLE

pubs.acs.org/IC

First-Principles Study of Lattice Dynamics and Thermodynamics of TiO_2 Polymorphs

Zhi-Gang Mei,* Yi Wang, Shun-Li Shang, and Zi-Kui Liu

Department of Materials Science and Engineering, The Pennsylvania State University, University Park, Pennsylvania 16802, United States

ABSTRACT: The structural, phonon, and thermodynamic properties of six TiO_2 polymorphs, i.e., rutile, anatase, columbite, baddeleyite, orthorhombic I, and cotunnite, have been systematically investigated by density functional theory. The predicted volumes, bulk modulus, and Debye temperature are in good agreement with experiments. The phonon dispersions of the TiO_2 polymorphs were studied by the supercell approach, whereas the long-range dipole−dipole interactions were calculated by linear response theory to reproduce the LO−TO splitting, making accurate prediction of phonon frequencies for the polar material TiO_2. The calculated phonon dispersions show that all TiO_2 polymorphs are dynamically stable at ambient pressure, indicating the high-pressure phases might be quenched to ambient conditions as ultrahard materials. Furthermore, the finite temperature thermodynamic properties of TiO_2 polymorphs were predicted accurately from the obtained phonon density of states, which is critical in the future study of the pressure−temperature phase diagram of TiO_2. The calculated Gibbs energies reveal that rutile is more stable than anatase at ambient pressure. We derived the Gibbs energy and heat capacity functions for all TiO_2 polymorphs for use in thermodynamic modeling of phase equilibria.

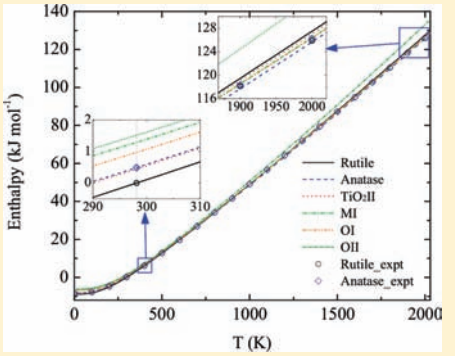

1. INTRODUCTION

Titanium dioxide (TiO_2) possesses a rich phase relation with many polymorphs. Among them, rutile ($P4_2/mnm$), anatase ($I4_1/amd$), and brookite ($Pbca$) are naturally occurring phases. Because of its high refractive index (2.7)[1] and wide band gap (~3.0 eV),[2] TiO_2 shows a wide range of potential applications in areas such as white pigments, high-efficiency solar cells,[3] photocatalysts,[4] and storage capacitors in dynamic random access memories.[5] Among the polymorphs, the rutile phase has been extensively studied from both experimental and theoretical perspectives, thanks to the availability of good single crystals for characterization. Recently, researchers have focused on the anatase phase due to its promising photochemical and photoelectrochemical applications.[6,7] Additionally, nanostructured TiO_2 has attracted significant interest as a host material for its unique physical and chemical properties.[8]

Many of the technologically important properties of TiO_2 are closely related to the lattice dynamics of the crystal. Information about its chemical bonding, elastic behavior, specific heat, dielectric behavior, and optical properties can be obtained from the analysis of the phonon dispersion relation. For example, the exceptionally high static dielectric constant of rutile and its anomalous increase as temperature decreases can be understood by the softening of the transverse optic A_{2u} mode, which may result in ferroelectric phase transitions.[9] The full phonon dispersion relation of rutile TiO_2 has been studied by Traylor et al. using coherent neutron inelastic scattering along the principal directions in the Brillouin zone.[10] The phonon frequencies at Γ point were also measured by Raman[11] and infrared spectroscopies.[12] However, there are very few papers dealing with the phonon spectra of the anatase phase,[13−15] owing to the scarcity of good quality single crystals for measurement. Although the lattice dynamics of the rutile and anatase phases have been studied by several authors using first-principles calculations,[9,15−21] very few papers dealt with their full phonon dispersion relations.

At elevated pressures, TiO_2 experiences a series of structural phase transitions. Its high-pressure polymorphs, i.e., columbite (TiO_2 II phase, space group $Pbcn$),[22] baddeleyite (MI, $P2_1/c$),[23] orthorhombic I (OI, $Pbca$),[24] and cotunnite (OII, $Pnma$),[25] were discovered at increased pressures. The cotunnite-structured TiO_2 was reported to be the hardest oxide ever known.[25] Recently, cubic TiO_2 was synthesized at high pressures and temperatures, which may serve as an important promising material for future generation solar cells.[26] To date, there are very few studies of the phonon properties of the high-pressure polymorphs of TiO_2.[18] Phonon density of states (DOS), however, are of critical importance to the study of Helmholtz and Gibbs energies, phase stabilities, and pressure−temperature phase diagrams,[27] which could be useful in identifying the proper synthesis conditions for the potential ultrahard TiO_2 phases.

The present work aims at providing a systematic study of the structural, phonon, and thermodynamic properties of six TiO_2 polymorphs, i.e., rutile, anatase, TiO_2II, MI, OI, and OII, by first-

Received: February 18, 2011
Published: June 29, 2011

ACS Publications © 2011 American Chemical Society

principles density functional theory (DFT) calculations. The first-principles study of the vibrational modes in TiO_2 polymorphs is thus expected to give a firm baseline for the properties of nanosized phases. The Gibbs energy functions derived from the first-principles calculations can be used for the calculation of phase diagram (CALPHAD) thermodynamic modeling of the complex oxide system.[28] The rest of this paper is organized as follows. In section 2, the theories for the calculations of phonon and thermodynamic properties are outlined. In section 3, the details for the first-principles total energy and phonon calculations are presented. In section 4, we discuss the obtained properties of TiO_2 polymorphs, including (i) the equilibrium structural properties, (ii) the phonon dispersion relations and phonon DOS's, and (iii) the thermodynamic properties. Finally, the conclusions of this work are given in section 5.

2. THEORY

The phonon frequencies can be obtained by solving the eigenvalue problem of the reciprocal dynamic matrix $\tilde{D}$[29]

$$\omega^2(\mathbf{q},l)\mathbf{e}(\mathbf{q},l) = \tilde{D}(\mathbf{q})\mathbf{e}(\mathbf{q},l) \quad (1)$$

where $\omega(\mathbf{q},l)$ is the phonon frequency with respect to wave vector $\mathbf{q}$ and phonon mode l and $\mathbf{e}(\mathbf{q},l)$ the corresponding normalized atomic displacement weighted by the square root of the atomic mass. The dynamical matrix $\tilde{D}$ is related to the real-space force constant Φ by the following Fourier transformation[29]

$$\tilde{D}^{jk}_{\alpha\beta}(\mathbf{q}) = \frac{1}{\sqrt{\mu_j\mu_k}}\frac{1}{N}\sum_P \Phi^{jk}_{\alpha\beta}(0,P)exp\{i\mathbf{q}\cdot[\mathbf{R}(P)-\mathbf{R}(0)]\} \quad (2)$$

where α and β are the Cartesian axes of either x, y, or z, j and k are the indices of atoms in the primitive cell, μ_j is the atomic mass of the jth atom in the primitive cell, N is the number of primitive unit cells in the supercell, and $\mathbf{R}(P)$ is the position of the Pth primitive cell in the supercell.

For accurate predictions of phonon frequencies of polar material TiO_2, it is critical to consider the long-range dipole−dipole interactions in order to study the LO−TO splitting presented in TiO_2. The effects of dipole−dipole interactions are incorporated into the dynamic matrix through the long-range contributions to the force constants[30]

$$\Phi^{jk}_{\alpha\beta}(0,P) = \phi^{jk}_{\alpha\beta}(0,P) + \varphi^{jk}_{\alpha\beta} \quad (3)$$

where $\phi^{jk}_{\alpha\beta}$ is the cumulative contribution from short-range interactions and $\varphi^{jk}_{\alpha\beta}$ the contribution from long-range interactions due to the dipole−dipole effect. We find that $\varphi^{jk}_{\alpha\beta}$ can be explicitly expressed as follows[30]

$$\varphi^{jk}_{\alpha\beta} = \frac{1}{N}\frac{4\pi e^2}{V}\frac{[\mathbf{q}\cdot\mathbf{Z}^*(j)]_\alpha[\mathbf{q}\cdot\mathbf{Z}^*(k)]_\beta}{\mathbf{q}\cdot\boldsymbol{\varepsilon}_\infty\cdot\mathbf{q}} \quad (4)$$

where V is the volume of the primitive unit cell, $\mathbf{Z}^*(j)$ is the Born effective charge tensor of the jth atom in the primitive unit cell, and $\boldsymbol{\varepsilon}_\infty$ is the high-frequency static dielectric tensor, i.e., the contribution to the dielectric permittivity tensor from the electronic polarization. Because of the long-range dipole−dipole interactions, i.e., the contribution of the nonanalytical part to the dynamic matrix is a Fourier transformation of force constants in the limit of zero wavevector, an inverse Fourier transformation of the nonanalytical part of dynamic matrix gives the real-space force constants shown in eq 4 as the zero-order term. The force constants from long-range interaction, $\varphi^{jk}_{\alpha\beta}$ in eq 3, can be calculated in reciprocal space by linear response theory, and $\phi^{jk}_{\alpha\beta}$ can be obtained from the supercell approach in real space.[30] The summation of these two contributions provides the interpolation in real space between the finite size of the supercell and the infinite point derived from the limit of zero wavevector. This approach thus makes full use of the accuracies of the force constants calculated in real space and the dipole−dipole interactions calculated in reciprocal space and accordingly avoid the semiempirical procedure for extrapolating the LO phonon frequencies for a general $\mathbf{q}$ point between the Brillouin zone center and the zone boundary for polar materials as developed by Parlinski[31] for the direct approach. The reliability of the current approach for phonon calculation has been verified by our recently published work for MnO and NiO,[32] $SrTiO_3$,[33] Sr_2RuO_4,[34] and $BiFeO_3$.[35]

Table 1. Details of the First-Principles Calculations of the Total Energy and Phonon Spectra of the TiO_2 Polymorphs, Including the Space Group, k-Point Mesh for Electronic Structure Calculations, and Supercell and k-Point Mesh for Phonon Calculations

		k-point mesh		k-point mesh
phase	space group	electron	supercell	phonon
rutile	$P4_2/mnm$	18 × 18 × 27	2 × 2 × 2	3 × 3 × 3
anatase	$I4_1/amd$	19 × 19 × 7	3 × 3 × 3	3 × 3 × 3
TiO_2II	$Pbcn$	16 × 13 × 14	2 × 2 × 2	3 × 3 × 3
MI	$P2_1/c$	13 × 12 × 12	2 × 2 × 2	3 × 3 × 3
OI	$Pbca$	7 × 12 × 13	1 × 2 × 2	3 × 3 × 3
OII	$Pnma$	12 × 10 × 20	2 × 2 × 2	3 × 3 × 3

The Helmholtz energy (F) of a system at volume V and temperature T can be approximated as[27]

$$F(V,T) = E_0(V) + F_{vib}(V,T) \quad (5)$$

where E_0 is the 0 K static energy at volume V and F_{vib} the vibrational free energy estimated from phonon DOS.[29] The equilibrium free energy F at each temperature T can be obtained by minimizing eq 5 with respect to V.

3. COMPUTATIONAL DETAILS

The DFT-based first-principles calculations were performed by the projector-augmented wave method[36] as implemented in the Vienna ab initio simulation package (VASP).[37,38] The local density approximation (LDA) was utilized to depict the exchange-correlation functional due to its capabilities to give an overall better description of the properties studied in this work for TiO_2 than the generalized gradient approximations (GGA). Dense k-point meshes in the first Brillouin zone were utilized (see Table 1). The cell shapes and ionic positions of TiO_2 phases are fully relaxed by the Gaussian smearing technique. Accurate total energy calculations are performed by means of the linear tetrahedron method with Blöchl's correction.[39] In all cases the total energies are converged to 10^{-7} eV/cell with an energy cutoff of 500 eV.

The phonon properties of TiO_2 polymorphs were studied by the supercell approach as implemented in Yphon code.[30] The Born effective charge tensor and electronic dielectric constant tensor were calculated using the linear-response method as

dx.doi.org/10.1021/ic200349p |Inorg. Chem. 2011, 50, 6996–7003

Table 2. Calculated Properties of the TiO_2 Polymorphs at 0 K (without considering the zero-point vibrations) and 298 K Together with the Experimental Data, Including the Equilibrium and High-Pressure Lattice Parameters (a, b, c) and Volume (V), Bulk Modulus (B), and Debye Temperature (Θ_D)

phase	reference	T (K)	P (GPa)	a, b, c (Å)	V (Å^3/TiO_2)	B (GPa)	Θ_D (K)
rutile	this work	0	0		30.64	250	809[a]
	this work	298	0	4.593, 4.593, 2.935	30.96	241	
	expt.	298	0	4.593, 4.593, 2.959[c]	31.2[b], 31.21[c]	211 ± 7,[d] 235 ± 10[b]	778[e]
anatase	this work	0	0		33.58	185	834[a]
	this work	298	0	3.759, 3.759, 9.585	33.86	175	
	expt.	298	0	3.785, 3.785, 9.512[c]	34.07[c,f]	179 ± 2[f]	
TiO_2II	this work	0	0		30.06	245	823[a]
	this work	298	0	4.536, 5.486, 4.883	30.37	240	
	this work	298	13.2	4.465, 5.383, 4.805	28.88		
	expt.	298	0	4.541, 5.493, 4.906[f]	30.53[b], 30.59[f]	253 ± 12,[b] 258 ± 8[f]	
	expt.	298	13.2	4.401, 5.382, 4.864[g]	28.8[g]		
MI	this work	0	0		28.02	207	873[a]
	this work	298	0		28.31	203	
	this work	298	19.1	4.583, 4.799, 4.744	26.09		
	expt.	298	0		28.06[b,f]	290 ± 10,[f] 298 ± 21[b]	
	expt.	298	19.1	4.602, 4.855, 4.751[g]	26.28[g]		
OI	this work	0	0		27.01	274	893[a]
	this work	298	0		27.29	269	
	this work	298	28.7	8.975, 4.811, 4.586	24.75		
	expt.	298	0		27.27[h], 27.54[b]	314 ± 16,[b] 318 ± 3[h]	
	expt.	298	28.7	9.014, 4.835, 4.616[g]	25.15[g]		
OII	this work	0	0		24.44	287	884[a]
	this work	298	0		24.74	273	
	this work	298	59.6	5.011, 5.880, 2.906	21.41		
	expt.	298	0		25.10[g], 25.28[b]	306 ± 9,[g] 312 ± 34[b]	
	expt.	298	59.6	5.028, 5.889, 2.930[g]	21.67[g]		

[a] Estimated from the second-moment Debye cutoff frequency obtained by phonon DOS. [b] Reference 48. [c] Reference 49. [d] Reference 52. [e] Reference 54. [f] Reference 50. [g] Reference 51. [h] Reference 24.

implemented in VASP 5.2.[40] To calculate force constants, we used an energy cutoff of 400 eV and a 3 × 3 × 3 k-point mesh for the supercells. Ancillary calculations using denser k-point mesh and larger supercell, such as 5 × 5 × 5 k-point mesh and 3 × 3 × 3 supercell, were tested for the phonon properties of the rutile phase; however, no significant difference was found. All the calculated force constants within the supercell were used for the real-space component of the force constants. More details about the first-principles total energy and phonon calculations are shown in Table 1, including space group, k-point mesh for electronic structure calculations, supercell size, and k-point mesh for force constants calculations.

4. RESULTS AND DISCUSSION

In this section, the predicted equilibrium and high-pressure lattice parameters, volumes, bulk moduli, Debye temperatures, phonon dispersion relations and DOS, and finite temperature thermodynamic properties of the TiO_2 polymorphs are presented and compared with the experimental data when available.

4.1. Structural Properties. The total energies of the six polymorphs of TiO_2 calculated at 10 different volumes in the present work are fitted by the third-order Birch−Murnaghan equations.[41,42] The obtained 0 K equilibrium properties, including the lattice parameters, volume (V), bulk modulus (B), and Debye temperature (Θ_D), are listed in Table 2. Similar to other DFT calculations,[43−47] our 0 K LDA calculations (without considering the zero-point vibrations) underestimate the equilibrium V of TiO_2 polymorphs with errors less than 1.8%,[24,48−51] except for 2.5% of the cotunnite phase.[48,51] Accordingly, the bulk moduli of rutile and anatase TiO_2 are overestimated by 6.4% and 3.4%, respectively.[48,50,52] As for the high-pressure polymorphs of TiO_2, the bulk moduli are much underestimated,[24,48−51] especially for the MI phase.[48,49] Nevertheless, our calculations are consistent with most of the recent DFT calculations.[45−47] The reason for the underestimation could be due to the difficulty for the high-pressure measurements, since we noticed that the uncertainties for the measured bulk moduli of the high-pressure phases are relatively large (see Table 2). From the calculated phonon DOS, we estimated the Debye temperature using the second-moment Debye cutoff frequency.[53] Similar to bulk modulus, Debye temperature is intimately related to the bonding strength in a material. The predicted Θ_D of the rutile phase is very close to the experimental value at high temperatures estimated from the heat capacity measurements.[54] Additionally, our calculations show that the high-pressure polymorphs have relatively larger Θ_D than the ambient stable ones, indicating stronger bonding in these phases, in agreement with the calculated force constants (not shown here).

For more realistic comparison with the experimental data, we estimated the equilibrium structural properties at 298 K since

dx.doi.org/10.1021/ic200349p |Inorg. Chem. 2011, 50, 6996–7003

Table 3. Comparison of the Computed Phonon Frequencies (in THz) at the Γ Point with the Experimental Data for Rutile TiO_2

mode	this work	optical[a]	neutron[b]	theory[c]	theory[d]	theory[e]	theory[f]	theory[g]
A_{1g}	18.72	18.36	18.30	18.46	18.30	18.66	18.67	18.50
A_{2g}	12.39			12.38		12.46	12.66	12.20
B_{1g}	4.04	4.29	4.25	3.96	4.25	3.75	3.95	3.45
B_{2g}	25.05	24.78	24.72	24.02	24.72	24.82	24.90	24.67
E_g	14.21	13.41	13.34	14.16	13.89	14.13	14.18	14.06
$B_{1u}^{(1)}$	3.75		3.39	3.53	3.12	3.50	3.33	3.36
$B_{1u}^{(2)}$	12.43		12.18	12.52	11.78	12.22	12.12	12.02
A_{2u}(TO)	5.97	5.01	5.18	5.74	4.63	5.28	4.72	4.92
E_u^1(TO)	5.26	5.49	5.66	4.31	5.74	4.94	4.88	4.38
E_u^2(TO)	11.83	11.64		11.79	11.51	11.73	11.74	11.63
E_u^3(TO)	15.15	15.00	14.81	14.95	14.64	14.77	14.92	14.54
A_{2u}(LO)	24.51	24.33		24.02		23.06	22.82	22.81
E_u^1(LO)	10.52	11.19	11.23	10.57		10.54	10.72	10.22
E_u^2(LO)	13.44	13.74	12.85	13.04		13.24	13.27	13.16
E_u^3(LO)	23.81	24.18	25.24	23.63		24.23	24.09	24.07

[a] Measured by Raman[11] and infrared[12] spectroscopies. [b] Reference 10. [c] Reference 17. [d] Reference 9. [e] Reference 16. [f] Reference 20. [g] Reference 21.

Table 4. Comparison of the Computed Phonon Frequencies (in THz) at the Γ Point with the Experimental Data for Anatase TiO_2

mode	this work	Raman[a]	Raman[b]	Raman[c]	infrared[d]	theory[a]	theory[e]	theory[f]
$E_g^{(1)}$	3.15	4.29	4.32	4.32		4.70	4.37	4.22
$E_g^{(2)}$	4.95	5.94	5.91	5.91		5.71	5.13	4.92
$B_{1g}^{(1)}$	13.94	11.84	11.99	11.96		11.41	11.94	11.71
$B_{1g}^{(2)}$	15.54	15.35	15.44	15.56		15.60	15.54	15.18
A_{1g}	16.05	15.53	15.56	15.38		15.55	16.07	15.83
$E_g^{(3)}$	19.64	19.16	19.19	19.16		19.21	19.85	19.50
E_u^1(LO)	7.19				7.85	7.87	7.45	7.30
E_u^1(LO)	9.76				10.97	10.63	10.21	10.21
A_{2u}(TO)	12.05				11.00	10.00	11.25	10.55
A_{2u}(LO)	22.67				22.63	21.90	22.28	21.85
E_u^2(LO)	13.95				13.04	12.96	14.39	13.77
E_u^2(TO)	26.67				26.26	26.35	26.75	26.38
B_{2u}	17.20					16.25	16.93	16.66

[a] Reference 15. [b] Reference 55. [c] Reference 13. [d] Reference 14. [e] Reference 19. [f] Reference 20.

most of the measurements were carried out at room temperature. The predicted equilibrium volume and bulk modulus at 298 K are tabulated in Table 2. By taking account of the lattice vibrational contribution, the estimated equilibrium volumes agree much better with experiments than the 0 K calculations do and the average of the relative errors decreases from 1.4% to 0.4%. The same conclusion applies to the bulk moduli of rutile and anatase TiO_2, with the average of the relative errors reducing from 5% to 2.4%. However, consideration of the phonon contribution does not help to improve the bulk moduli of the high-pressure phases. For the cotunnite-structured TiO_2, our predicted bulk modulus is much smaller than the value reported by Dubrovinsk et al.[25] but agrees with recent experiments[48,51] and theoretical investigations.[45−47] Since the experimental equilibrium volume and bulk modulus of the high-pressure polymorphs are estimated from the equation of state fitting, it is more meaningful to compare our predictions with the direct measurements, e.g., high-pressure volumes. The predicted high-pressure volumes agree very well with the experimental data for all the high-pressure polymorphs (see Table 2 for more details).[51] The average of the relative errors is less than 0.8%, indicating the reliability of our calculations at high pressures.

4.2. Phonon properties. For the rutile phase, there are 6 atoms in the primitive cell; thus, there should be 15 optical modes and three acoustic modes. From the group analysis of its space group ($P4_2/mnm$), the optical modes at the Γ point belong to the following irreducible representations

$$\Gamma_{opt}(\text{rutile}) = A_{1g} + A_{2g} + A_{2u} + B_{1g} + 2B_{1u} + B_{2g} + E_g + 3E_u \quad (6)$$

The symbol g represents Raman active, u infrared active, and E degenerate. In principle, the long-range dipole−dipole interactions in the ionic compounds can result in the LO−TO splitting (longitudinal and transversal optical phonon frequencies). The LO−TO splitting occurs at the Γ point and only for infrared active modes. Since A_{2u} and E_u modes are polar, they split into LO and TO modes with different frequencies due to macroscopic electric fields associated with the LO phonons. A_{2g} and B_{1u} modes, however, are Raman and infrared inactive (silent modes).

dx.doi.org/10.1021/ic200349p |Inorg. Chem. 2011, 50, 6996–7003

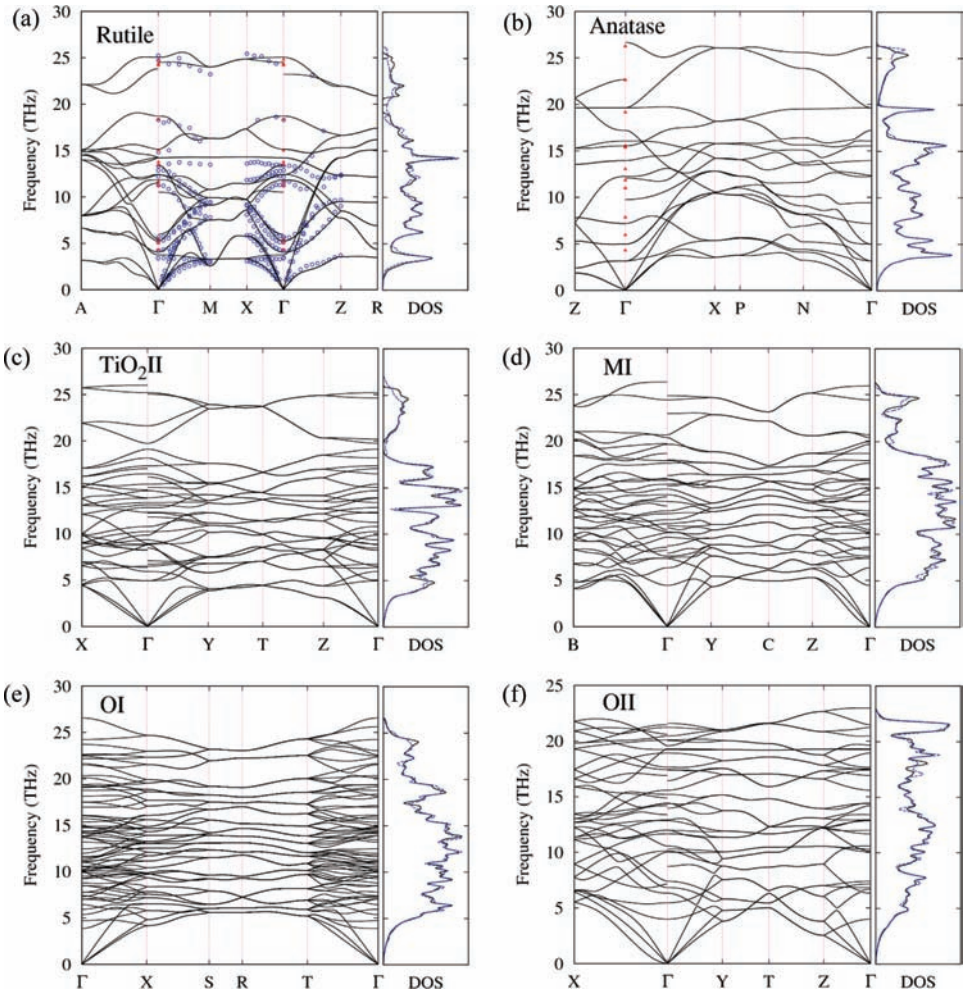

Figure 1. Phonon dispersion relations and phonon density of states (DOS) of the TiO_2 polymorphs, i.e., rutile, anatase, TiO_2II, MI, OI, and OII. The solid lines represent the present calculated phonon spectra, the open circles (blue) are the inelastic neutron scattering data,[10] and the solid red triangles are Raman[11] or infrared data.[12] Black solid and blue dashed lines represent phonon DOS with and without dipole−dipole interactions, respectively.

In Table 3, we compare the calculated Γ-point phonon frequencies of the rutile phase with the experimental neutron scattering, infrared, and Raman measurements,[10−12] together with other calculations.[9,16,17,20,21] The optical phonon frequencies at Γ point are accurately predicted, and all the LO−TO splittings are also correctly reproduced. The relative errors for most of the phonon modes are very small, less than 6%, except for the low-frequency mode A_{2u}(TO).

Similar to the rutile phase, there are 6 atoms in the primitive cell of the anatase phase; thus, there should be 15 optical modes. From the group analysis of its space group ($I4_1/amd$), the optical modes at the Γ point belong to the following irreducible representations

$$\Gamma_{opt}(\text{anatase}) = A_{1g} + A_{2u} + 2B_{1g} + B_{2u} + 3E_g + 2E_u \qquad (7)$$

A_{1g}, B_{1g}, and E_g are Raman active, while A_{2u} and E_u are infrared active. B_{2u} is a silent mode. The calculated phonon frequencies at Γ point for the anatase phase are summarized in Table 4, along with the experimental and other theoretical results.[13−15,19,20,SS] The agreement with experiments seems not as good as other calculations, since theoretical equilibrium lattice parameters, rather than experimental values, were adopted for the phonon calculations in order to achieve a complete first-principles prediction. Using the experimental lattice parameters of anatase, the overall agreement improves substantially.

In the meanwhile, we studied the full phonon dispersion relations throughout the whole Brillouin zone and plotted the phonon DOS's for all TiO_2 polymorphs at their theoretic equilibrium volumes, as shown in Figure 1. To date, only the phonon dispersion relation of the rutile phase has been measured in the whole Brillouin zone by the coherent neutron inelastic scattering method.[10] The presently predicted phonon modes of rutile TiO_2 agree well with the experimental data at both low and high frequencies and show an overall improvement over other theoretical calculations[17,20,21] using the current mixed-space approach to the phonon calculations. In Figure 1, we also compared the phonon DOS's of the TiO_2 polymorphs with and without dipole−dipole interactions. The effect of dipole−dipole interaction on the whole shape of the phonon DOS is small, especially at low frequencies, and the most notable changes appear at high frequencies. Thus, the dipole−dipole effect is important in the study of free energies and phase stabilities only at high temperatures. For the high-pressure polymorphs of TiO_2, it is very encouraging to discover that there is no imaginary phonon frequency in their phonon dispersions and DOS's,

dx.doi.org/10.1021/ic200349p |Inorg. Chem. 2011, 50, 6996–7003

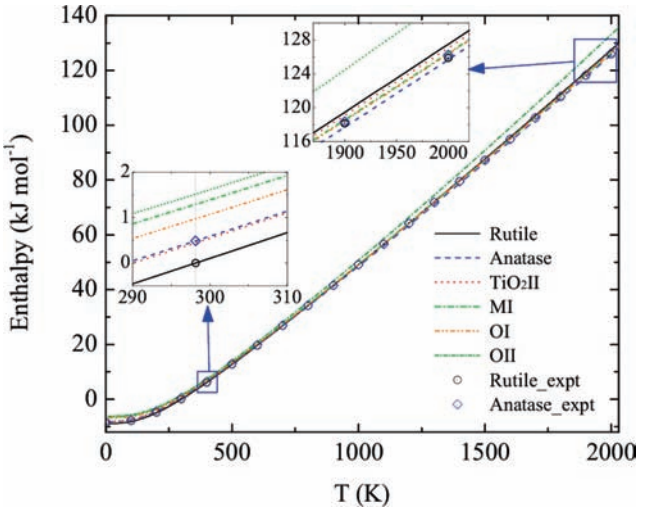

Figure 2. Enthalpies of the TiO_2 polymorphs, i.e., rutile, anatase, TiO_2II, MI, OI, and OII, with the enthalpy of rutile phase at 298.15 K and 1 atm as the reference. The lines represent the present calculations, and the open symbols are the critically evaluated values obtained by Chase et al.[56] The inserts are the magnified plots with temperatures around 298 and 1950 K, respectively.

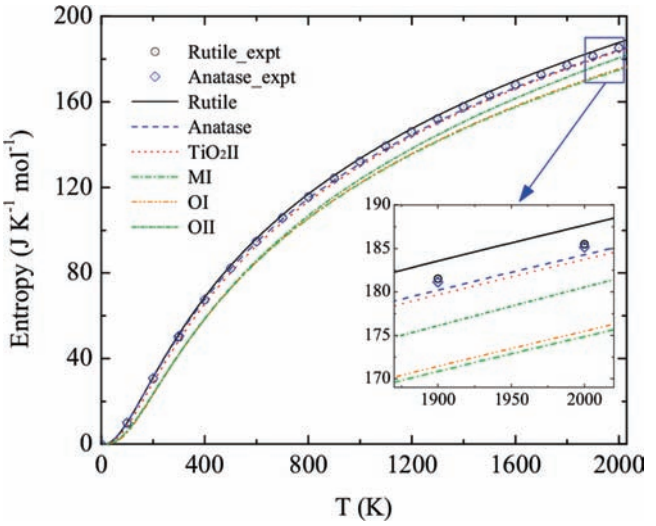

Figure 3. Entropies of the TiO_2 polymorphs, i.e., rutile, anatase, TiO_2II, MI, OI, and OII. The lines represent the present calculations, while the open symbols are the critically evaluated values obtained by Chase et al.[56] The insert is the magnified plot with temperature around 1950 K.

indicating that they are dynamically stable under ambient pressure. It suggests that the high-pressure polymorphs of TiO_2 can be quenched to the ambient conditions as metastable phases, which means that cotunnite TiO_2 might be stabilized at ambient pressure as an ultrahard material.

4.3. Thermodynamic Properties. With the obtained phonon DOS's at six different volumes in the present work, the Helmholtz energy (F) of TiO_2 polymorphs can be evaluated based on the quasi-harmonic approximation, i.e., eq 5. Accordingly, the entropy (S) and internal energy (U) can be estimated by the following equations

$$S = -\left(\frac{\partial F}{\partial T}\right)_V \tag{8}$$

$$U = F - TS = F - T\left(\frac{\partial F}{\partial T}\right)_V \tag{9}$$

Neglecting the influence of pressure (P) on the solid phases (i.e., the PV term), the internal energy is equal to the enthalpy (H) and the Helmholtz free energy (F) is equal to the Gibbs energy (G). We calculated H and S as a function of temperature up to the melting temperature (T_m = 2130 K)[56] for rutile, anatase, TiO_2 II, MI, OI, and OII TiO_2, where the rutile phase at 298.15 K and 1 atm was chosen as the reference state for H. As shown in Figures 2 and 3, the predicted H and S of rutile and anatase TiO_2 are in excellent agreement with the critically evaluated values by Chase et al. from experiments.[56] For rutile phase, H and S are somewhat overestimated at high temperatures. However, the differences from experiments are very small even at 2000 K, which is less than 1.2% for both H and S, while for anatase phase the enthalpy and entropy are a little underestimated at high temperatures, with relative errors of 0.4% and 0.5% for H and S, respectively. We notice that OII TiO_2 shows a relatively large slope of H compared with other phases, especially at high temperatures. Since the slope of enthalpy with respect to temperature equals heat capacity, OII TiO_2 should have the

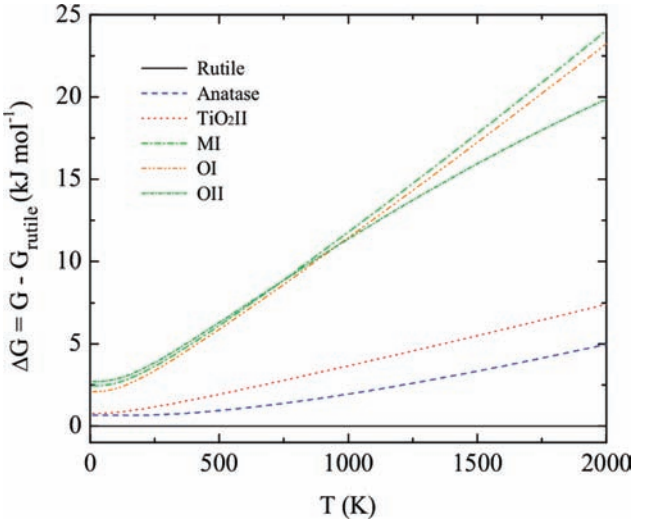

Figure 4. Calculated Gibbs energy differences ($\Delta G = G - G_{rutile}$) of the TiO_2 polymorphs as a function of temperature with respect to rutile phase.

largest heat capacity among all TiO_2 phases, which is verified by the following heat capacity calculations.

To compare the phase stabilities of TiO_2, we also plotted the Gibbs energy difference as a function of temperature with respect to the rutile phase in Figure 4. There have been a lot of debates about the relative stabilities of rutile and anatase phases under ambient conditions. A number of first-principles studies have been performed to address this issue in the past decade, and recent calculations predicted anatase to be more stable than rutile at 0 K and ambient pressure.[46,47,57] However, the lattice stability at finite temperature and ambient pressure is determined by the Gibbs energy rather than internal energy. Although our 0 K calculations do reveal that anatase has lower total energy than rutile, the rutile phase should be more stable than anatase when considering the zero-point vibrations. Furthermore, the finite

dx.doi.org/10.1021/ic200349p |*Inorg. Chem.* 2011, 50, 6996–7003

Table 5. Gibbs Energy Functions (G) of the TiO_2 Polymorphs at Ambient Pressure

phase	Gibbs energy function (G) (298.15 K < T < T_m = 2130 K)
rutile	$-27\,598 + 448.1T - 72.92T\ln T - 2.10 \times 10^{-3}T^2 + 8.43 \times 10^{5}T^{-1}$
anatase	$-26\,351 + 435.7T - 70.99T\ln T - 2.31 \times 10^{-3}T^2 + 8.15 \times 10^{5}T^{-1}$
TiO_2II	$-27\,472 + 451.8T - 72.97T\ln T - 1.92 \times 10^{-3}T^2 + 8.90 \times 10^{5}T^{-1}$
MI	$-27\,328 + 457.8T - 72.71T\ln T - 1.80 \times 10^{-3}T^2 + 9.88 \times 10^{5}T^{-1}$
OI	$-27\,478 + 459.3T - 72.98T\ln T - 1.72 \times 10^{-3}T^2 + 9.72 \times 10^{5}T^{-1}$
OII	$-26\,799 + 452.0T - 71.72T\ln T - 3.86 \times 10^{-3}T^2 + 9.81 \times 10^{5}T^{-1}$

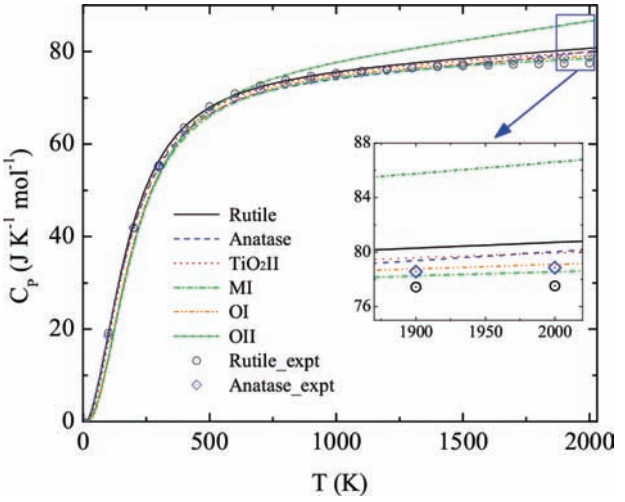

Figure 5. Heat capacities of the TiO_2 polymorphs, i.e., rutile, anatase, TiO_2II, MI, OI, and OII. The lines represent the present calculations; the open symbols are the critically evaluated values obtained by Chase et al.[56] The insert is the magnified plot with temperature around 1950 K.

Table 6. Heat Capacity Functions (C_P) of the TiO_2 Polymorphs at Ambient Pressure

phase	heat capacity function (C_P) (298.15 K < T < T_m = 2130 K)
rutile	$72.92 + 4.20 \times 10^{-3}T - 1.69 \times 10^{6}T^{-2}$
anatase	$70.99 + 4.61 \times 10^{-3}T - 1.63 \times 10^{6}T^{-2}$
TiO_2II	$72.97 + 3.84 \times 10^{-3}T - 1.78 \times 10^{6}T^{-2}$
MI	$72.71 + 3.61 \times 10^{-3}T - 1.98 \times 10^{6}T^{-2}$
OI	$72.98 + 3.44 \times 10^{-3}T - 1.94 \times 10^{6}T^{-2}$
OII	$71.72 + 7.72 \times 10^{-3}T - 1.96 \times 10^{6}T^{-2}$

temperature Gibbs energy study predicts that rutile is more stable than anatase in the whole temperature range we studied, as shown in Figure 4. We also see that the Gibbs energies of the high-pressure polymorph TiO_2II are close to those of anatase at low temperatures, which explains why the TiO_2II phase was often observed as metastable pressure-quenched phases at ambient pressure instead of anatase.[23,48] For use in CALPHAD thermodynamic modeling, the following function is used to describe the Gibbs energies of the TiO_2 polymorphs from room temperature up to T_m, in per mole of formula unit[28]

$$G = a + bT + cT\ln T + dT^2 + eT^{-1} \quad (10)$$

where a, b, c, d, and e are fitting parameters. The derived Gibbs energy functions of all TiO_2 polymorphs are tabulated in Table 5.

The heat capacity at constant volume (C_V) can be calculated directly by

$$C_V = \left(\frac{\partial U}{\partial T}\right)_V = -T\left(\frac{\partial^2 F}{\partial T^2}\right)_V \quad (11)$$

The heat capacities measured at constant pressures (C_P) can be evaluated by the thermodynamic relation between C_V and C_P, $C_P - C_V = \alpha^3 VBT$, where α is the calculated thermal expansion coefficient (not shown in this work). Figure 5 shows the predicted C_P together with the available experimental data.[56] Our calculations reproduce the C_P of anatase TiO_2 very well in the whole temperature range, with a relative error of about 1.5% at 2000 K. The C_P of rutile TiO_2 is somewhat overestimated, especially above 1200 K; however, the relative error at 2000 K is less than 4%. The difference might be traced back to the stability of the rutile phase above 1200 K. Since heat capacity is a second derivative of free energy with respect to temperature, it is more demanding on the accuracy of free energy than entropy and enthalpy do. Thus, the presently predicted C_P of the rutile phase is still acceptable. For the high-pressure OII phase, it shows an abnormally large heat capacity at high temperatures compared with other TiO_2 phases, consistent with the above analysis of the enthalpies. We also derived the heat capacity functions for all TiO_2 polymorphs by the formula $C_P = -c - 2dT - 2eT^{-2}$, valid from room temperature to T_m, shown in Table 6.

5. SUMMARY

We studied the structural, phonon, and thermodynamic properties of the six polymorphs of TiO_2, i.e., rutile, anatase, TiO_2II, MI, OI, and OII, by DFT calculations. Our 0 K LDA calculations predicted the equilibrium volumes of TiO_2 polymorphs very well, except for the cotunnite phase. By taking the lattice vibrations at finite temperatures into account, the agreement improves substantially. The bulk moduli of rutile and anatase TiO_2 calculated at room temperature agree with the experimental data, while those of the high-pressure polymorphs are underestimated. The calculated Debye temperatures indicate that the atomic bondings in the high-pressure polymorphs are stronger than those in the rutile and anatase phases, in agreement with the calculated force constants. We predicted the phonon frequencies at Γ point in the Brillouin zone for both rutile and anatase TiO_2, which are comparable to the experimental and other theoretical studies. The phonon dispersion relations along the high-symmetry directions in the Brillouin zone for all TiO_2 polymorphs have been predicted, and the LO−TO splittings are well reproduced for rutile and anatase phases by considering the dipole−dipole interactions. Additionally, we notice that there is no imaginary phonon frequency for all the high-pressure polymorphs, indicating that they are all mechanically stable at zero pressure. That means they might be quenched to ambient conditions as metastable phases. From the calculated phonon DOS, The finite temperature thermodynamic properties (enthalpy, entropy, Gibbs energy, and heat capacity) of all

dx.doi.org/10.1021/ic200349p |*Inorg. Chem.* 2011, 50, 6996–7003

TiO_2 polymorphs are predicted from the quasiharmonic phonon calculations, in excellent agreement with available experimental data. The calculated Gibbs energies reveal that rutile is more stable than anatase in the whole temperature range we studied. We derived the Gibbs energy and heat capacity functions for all TiO_2 polymorphs, which can be used in CALPHAD thermodynamic modeling of the oxide system.

AUTHOR INFORMATION

Corresponding Author
*E-mail: zzm108@psu.edu.

ACKNOWLEDGMENT

This work was funded by the TIE project of the Center for Computational Materials Design (CCMD), a National Science Foundation (NSF) Industry/University Cooperative Research Center through Grant IIP-0737759 and the National Science Foundation (NSF) through Grant No. DMR-1006557. First-principles calculations were carried out on the LION clusters supported by the Materials Simulation Center and the Research Computing and Cyber infrastructure unit at the Pennsylvania State University.

REFERENCES

(1) Li, J. G.; Ikeda, M.; Tang, C. C.; Moriyoshi, Y.; Hamanaka, H.; Ishigaki, T. *J. Phys. Chem. C* **2007**, *111*, 18018.
(2) Kavan, L.; Gratzel, M.; Gilbert, S. E.; Klemenz, C.; Scheel, H. J. *J. Am. Chem. Soc.* **1996**, *118*, 6716.
(3) Bach, U.; Lupo, D.; Comte, P.; Moser, J. E.; Weissortel, F.; Salbeck, J.; Spreitzer, H.; Gratzel, M. *Nature* **1998**, *395*, 583.
(4) Linsebigler, A. L.; Lu, G. Q.; Yates, J. T. *Chem. Rev.* **1995**, *95*, 735.
(5) Gan, J. Y.; Chang, Y. C.; Wu, T. B. *Appl. Phys. Lett.* **1998**, *72*, 332.
(6) Fujishima, A.; Honda, K. *Nature* **1972**, *238*, 37.
(7) Hadjiivanov, K. I.; Klissurski, D. G. *Chem. Soc. Rev.* **1996**, *25*, 61.
(8) Gleiter, H. *Prog. Mater. Sci.* **1989**, *33*, 223.
(9) Montanari, B.; Harrison, N. M. *Chem. Phys. Lett.* **2002**, *364*, 528.
(10) Traylor, J. G.; Smith, H. G.; Nicklow, R. M.; Wilkinson, M. K. *Phys. Rev. B* **1971**, *3*, 3457.
(11) Porto, S. P. S.; Fleury, P. A.; Damen, T. C. *Phys. Rev.* **1967**, *154*, 522.
(12) Eagles, D. M. *J. Phys. Chem. Solids* **1964**, *25*, 1243.
(13) Ohsaka, T.; Izumi, F.; Fujiki, Y. *J. Raman Spectrosc.* **1978**, *7*, 321.
(14) Gonzalez, R. J.; Zallen, R.; Berger, H. *Phys. Rev. B* **1997**, *55*, 7014.
(15) Giarola, M.; Sanson, A.; Monti, F.; Mariotto, G.; Bettinelli, M.; Speghini, A.; Salviulo, G. *Phys. Rev. B* **2010**, *81*, 174305.
(16) Lee, C.; Ghosez, P.; Gonze, X. *Phys. Rev. B* **1994**, *50*, 13379.
(17) Sikora, R. *J. Phys. Chem. Solids* **2005**, *66*, 1069.
(18) Kim, D. Y.; de Almeida, J. S.; Koci, L.; Ahuja, R. *Appl. Phys. Lett.* **2007**, *90*, 171903.
(19) Mikami, M.; Nakamura, S.; Kitao, O.; Arakawa, H. *Phys. Rev. B* **2002**, *66*, 155213.
(20) Shojaee, E.; Mohammadizadeh, M. R. *J. Phys.: Condens. Matter* **2010**, *22*, 015401.
(21) Mitev, P. D.; Hermansson, K.; Montanari, B.; Refson, K. *Phys. Rev. B* **2010**, *81*, 134303.
(22) Jamieson, J. C.; Olinger, B. *Science* **1968**, *161*, 893.
(23) Sato, H.; Endo, S.; Sugiyama, M.; Kikegawa, T.; Shimomura, O.; Kusaba, K. *Science* **1991**, *251*, 786.
(24) Dubrovinskaia, N. A.; Dubrovinsky, L. S.; Ahuja, R.; Prokopenko, V. B.; Dmitriev, V.; Weber, H. P.; Osorio-Guillen, J. M.; Johansson, B. *Phys. Rev. Lett.* **2001**, *87*, 275501.
(25) Dubrovinsky, L. S.; Dubrovinskaia, N. A.; Swamy, V.; Muscat, J.; Harrison, N. M.; Ahuja, R.; Holm, B.; Johansson, B. *Nature* **2001**, *410*, 653.
(26) Mattesini, M.; de Almeida, J. S.; Dubrovinsky, L.; Dubrovinskaia, N.; Johansson, B.; Ahuja, R. *Phys. Rev. B* **2004**, *70*, 212101.
(27) Mei, Z. G.; Shang, S. L.; Wang, Y.; Liu, Z. K. *Phys. Rev. B* **2009**, *80*, 104116.
(28) Liu, Z. K. *J. Phase Equilib. Diffus.* **2009**, *30*, 517.
(29) Dove, M. T. *Introduction to lattice dynamics*; Cambridge University Press: Cambridge, 1993.
(30) Wang, Y.; Wang, J. J.; Wang, W. Y.; Mei, Z. G.; Shang, S. L.; Chen, L. Q.; Liu, Z. K. *J. Phys.: Condens. Matter* **2010**, *22*, 202201.
(31) Parlinski, K.; Li, Z. Q.; Kawazoe, Y. *Phys. Rev. Lett.* **1997**, *78*, 4063.
(32) Wang, Y.; Saal, J. E.; Wang, J. J.; Saengdeejing, A.; Shang, S. L.; Chen, L. Q.; Liu, Z. K. *Phys. Rev. B* **2010**, *82*, 081104.
(33) Wang, Y.; Saal, J. E.; Mei, Z. G.; Wu, P. P.; Wang, J. J.; Shang, S. L.; Liu, Z. K.; Chen, L. Q. *Appl. Phys. Lett.* **2010**, *97*, 162907.
(34) Wang, Y.; Wang, J. J.; Saal, J. E.; Shang, S. L.; Chen, L. Q.; Liu, Z. K. *Phys. Rev. B* **2010**, *82*, 172503.
(35) Wang, Y.; Saal, J. E.; Wu, P.; Wang, J.; Shang, S.; Liu, Z.-K.; Chen, L.-Q. *Acta Mater.* **2011**, *59*, 4229.
(36) Blöchl, P. E. *Phys. Rev. B* **1994**, *50*, 17953.
(37) Kresse, G.; Furthmüller, J. *Phys. Rev. B* **1996**, *54*, 11169.
(38) Kresse, G.; Joubert, D. *Phys. Rev. B* **1999**, *59*, 1758.
(39) Blöchl, P. E.; Jepsen, O.; Andersen, O. K. *Phys. Rev. B* **1994**, *49*, 16223.
(40) Gajdos, M.; Hummer, K.; Kresse, G.; Furthmuller, J.; Bechstedt, F. *Phys. Rev. B* **2006**, *73*, 045112.
(41) Mei, Z.-G.; Shang, S.; Wang, Y.; Liu, Z.-K. *Phys. Rev. B* **2009**, *79*, 134102.
(42) Shang, S. L.; Saengdeejing, A.; Mei, Z. G.; Kim, D. E.; Zhang, H.; Ganeshan, S.; Wang, Y.; Liu, Z. K. *Comput. Mater. Sci.* **2010**, *48*, 813.
(43) Dewhurst, J. K.; Lowther, J. E. *Phys. Rev. B* **1996**, *54*, R3673.
(44) Swamy, V.; Muddle, B. C. *Phys. Rev. Lett.* **2007**, *98*, 035502.
(45) Koci, L.; Kim, D. Y.; de Almeida, J. S.; Mattesini, M.; Isaev, E.; Ahuja, R. *J. Phys.: Condens. Matter* **2008**, *20*, 345218.
(46) Ma, X. G.; Liang, P.; Miao, L.; Bie, S. W.; Zhang, C. K.; Xu, L.; Jiang, J. J. *Phys. Status Solidi B: Basic Solid State Phys.* **2009**, *246*, 2132.
(47) Wu, X. A.; Holbig, E.; Steinle-Neumann, G. *J. Phys.: Condens. Matter* **2010**, *22*, 295501.
(48) Al-Khatatbeh, Y.; Lee, K. K. M.; Kiefer, B. *Phys. Rev. B* **2009**, *79*, 134114.
(49) Burdett, J. K.; Hughbanks, T.; Miller, G. J.; Richardson, J. W.; Smith, J. V. *J. Am. Chem. Soc.* **1987**, *109*, 3639.
(50) Arlt, T.; Bermejo, M.; Blanco, M. A.; Gerward, L.; Jiang, J. Z.; Olsen, J. S.; Recio, J. M. *Phys. Rev. B* **2000**, *61*, 14414.
(51) Nishio-Hamane, D.; Shimizu, A.; Nakahira, R.; Niwa, K.; Sano-Furukawa, A.; Okada, T.; Yagi, T.; Kikegawa, T. *Phys. Chem. Miner.* **2010**, *37*, 129.
(52) Ming, L. C.; Manghnani, M. H. *J. Geophys. Res.* **1979**, *84*, 4777.
(53) Wolf, G. H.; Jeanloz, R. *Phys. Rev. B* **1985**, *32*, 7798.
(54) Pandey, H. N. *Phys. Status Solidi* **1965**, *11*, 743.
(55) Beattie, I. R.; Gilson, T. R. *Proc. R. Soc. London, Ser. A* **1968**, *307*, 407.
(56) Chase, M. W. *NIST-JANAF thermochemical tables*; American Institute of Physics: Washington, DC, 1998.
(57) Muscat, J.; Swamy, V.; Harrison, N. M. *Phys. Rev. B* **2002**, *65*, 224112.